Model-based Deep MR Imaging: the roadmap of generalizing compressed sensing model using deep learning

Jing Cheng[1], Haifeng Wang[1], Yanjie Zhu[1], Qiegen Liu[3], Xin Liu[1], Hairong Zheng[1], Leslie Ying[4], Dong Liang[1, 2]

[1] Paul C. Lauterbur Research Center for Biomedical Imaging, Shenzhen Institutes of Advanced Technology, Chinese Academy of Sciences, Shenzhen, Guangdong, China

[2] Research center for Medical AI, Shenzhen Institutes of Advanced Technology, Chinese Academy of Sciences, Shenzhen, Guangdong, China

Dong.Liang@siat.ac.cn

[3] Department of Electronic Information Engineering, Nanchang University, Nanchang, Jiangxi, China

[4] Departments of Biomedical Engineering and Electrical Engineering, University at Buffalo, the State University of New York, Buffalo, NY 14260 USA

1. Introduction

Accelerating magnetic resonance imaging (MRI) has been an ongoing research topic since its invention in the 1970s. Many researchers have been seeking for methods to increase imaging speed by reducing the amount of acquired k-space data. However, undersampling in k-space usually results in aliasing artifacts in reconstructions. Previous commercial proposals try to mitigate aliasing artifacts based on prior information [1-5]. For example, partial Fourier technique utilizes the conjugate symmetry property of k-space data [1]; parallel imaging benefits from the sensitivity information of multi-channel coils [2, 3]; and advanced compressed sensing (CS) uses sparsity prior either in image domain or some transform domains [4, 5]. Although these techniques have been applied to accelerate imaging speed in clinics, there are still some issues to address. For example, the acceleration factors of partial Fourier and parallel imaging methods are limited to a low level. CS-based methods can achieve high acceleration with theoretical guarantee. However, it is challenging to determine the numerical uncertainties in the reconstruction model such as the optimal sparse transformations, sparse regularizer in the transform domain, regularization parameters and the parameters of the optimization algorithm. Many attempts have been deliberated to solve these issues, such as some learning-based methods, e.g. dictionary learning [6, 7], and some numerical methods (e.g. L-curve [8], SURE[9]). However, there is no general strategy to overcome these shortcomings.

Recently, deep learning (DL) has been introduced in MR reconstruction and shown potential on significantly speeding up MR reconstruction [10-22]. In general, DL-MRI can be classified into two categories: data-driven methods and mode-driven methods. The data-driven DL methods adopt an end-to-end fashion to bypass the MR imaging model, by learning the map function between undersampled k-space/image and fully-sampled k-space/image, with the aid of a large training dataset [10-18]. Since its invention in 2016[10], requiring large size of training dataset and difficult to interpret have been becoming the challenges of data-driven DL methods. Some researchers tried another strategy by starting

from an established CS-MRI model, and unrolling the procedure of an iterative optimization algorithm to a network, while learning on the different level of variables: such as the regularization parameters, the regularization functions (transformation and regularizer), and even the data consistency metrics (i.e., learning the entire reconstruction model) [19-22]. As a result, such networks can perform well with smaller size of training sets and may be interpretable since it roots from the established reconstruction model.

However, the widespread application of model-based deep learning methods in MR reconstruction raises the following questions: 1. given an established CS model and an optimization algorithm, is there a general guideline on how to apply deep learning to achieve the best performance? 2. if unrolling all algorithms to the final state, will they lead to the same performance？ 3. is there difference on the required size of training set for different level of unrolling? In this paper, we try to answer these questions by proposing a general framework on combining the CS-MR model with deep learning, giving the examples to demonstrate the performance and requirements of different algorithms when improving the representative ability of prior information using deep learning.

2. Theory

2.1 MR reconstruction model

Generally, with linear gradient system and Cartesian sampling, the MR signal f can be formulated as following:

$$f = Am + \delta \qquad (1)$$

where m is the vector of pixels we wish to reconstruct from the data f, δ denotes the measurement errors which can be well modeled as gaussian noise, A is the encoding matrix. If Nyquist sampling criteria is met, then the MR image can be obtained directly by inverse Fourier transform. In fast MR imaging, the k-space data is usually acquired by sub-Nyquist sampling, then, the system matrix A is not well conditioned, and regularization is needed to reconstruct MR image. Thus the image reconstruction can be formulated as following optimization problem:

$$\hat{m} = \underset{m}{argmin} \frac{1}{2}\|Am - f\|_2^2 + \lambda\|\Psi m\|_{\mathrm{p}} \qquad (2)$$

$\|\Psi m\|_{\mathrm{p}}$ denotes the regularization term which can enforce prior information that improves image quality for undersampled data. In compressed sensing (CS), the sparsity prior is usually used as the regularization term, where Ψ is the sparse transform and $0 \le p \le 1$.

The regularized least-square objective function (2) is the best linear unbiased estimator (BLUE) but may not be the effective one to estimate the image $\hat{m}$ from the partial k-space data f. More generally, the reconstruction model can be written as

$$\hat{m} = \underset{m}{argmin}\, F(Am, f) + \lambda R(m) \qquad (3)$$

where $F(Am, f)$ denotes data fidelity, $R(m)$ is the regularization.

2.2 Model-driven Deep learning MRI approaches

Model-driven DL methods unroll the iterations of an optimization algorithm for reconstruction problem to a deep network, and learn the constraints and parameters in the reconstruction model from the training data. Thus, the network architectures of these approaches are determined by the data flow of the optimization algorithm. Specifically, starting from a traditional MR reconstruction model, ①we first relax the regularizations in the model and unroll the iterations of reconstruction to a learnable deep network architecture. ②Then, we further relax the constraints of data consistency in the model, let the network learn the data fidelity freely. ③Finally, the fixed structure of variables in the algorithm is broken and the combinations are learned by the network.

We will take three algorithms as examples to demonstrate the strategy from the specific reconstruction model and optimization algorithm to the learnable architecture step by step. The overall illustration of the algorithms and three learning states is summarized in Table 1.

Table 1. Summarization of the learning states with different algorithms.

learning state / algorithm	Ⅰ	Ⅱ	Ⅲ
PDHG-net	$R(m)$, $\|Am-f\|_2^2$	$R(m)$, $F(Am,f)$	$R(m), F(Am,f)$, variable combinations
ADMM-net	$\|\Psi(m)\|_p$, $\|Am-f\|_2^2$	$\|\Psi(m)\|_p$, $F(Am,f)$	$R(m), F(Am,f)$, variable combinations
ISTA-net	$\Psi(m)$, $\|Am-f\|_2^2$	$\Psi(m)$, $F(Am,f)$	$\Psi(m), F(Am,f)$, variable combinations

① the Primal Dual approach

PDHG-net- Ⅰ

The primal dual hybrid gradient algorithm, also known as Chambolle-Pock (CP) algorithm, has been applied on several image restoration problems such as de-noising, deconvolution, inpainting, etc [23]. The CP algorithm solves an optimization problem simultaneously with its dual, which provides a robust convergence check – the duality gap. Replacing $\|\Psi m\|_{\mathrm{p}}$ with $R(m)$, using the CP algorithm, the solution of problem (2) is

$$\begin{cases} d_{n+1} = prox_{\sigma}[F^*](d_n + \sigma A\bar{m}_n) \\ m_{n+1} = prox_{\tau}[R](m_n - \tau A^T d_{n+1}) \\ \bar{m}_{n+1} = m_{n+1} + \theta(m_{n+1} - m_n) \end{cases} \quad (4)$$

where σ, τ and θ are the algorithm parameters, F^* is the convex conjugate of the function $\frac{1}{2}\|Am-f\|_2^2$, and $prox$ denotes the proximal operator, which can be obtained by the following minimization:

$$prox_{\tau}[R](x) = \arg\min_z \left\{ R(z) + \frac{\|z-x\|_2^2}{2\tau} \right\} \quad (5)$$

Eq. (4) becomes

$$\begin{cases} d_{n+1} = \frac{d_n + \sigma(A\bar{m}_n - f)}{1+\sigma} \\ m_{n+1} = prox_{\tau}[R](m_n - \tau A^T d_{n+1}) \\ \bar{m}_{n+1} = m_{n+1} + \theta(m_{n+1} - m_n) \end{cases} \quad (6)$$

Since it is not easy to choose the optimal parameters and transforms, and the simplicity limitation of the convex functions that makes (5) have close-form solution is not always satisfied in practice, a learned operator Λ is used to replace the proximal operator $prox_{\tau}[R]$ and learn the parameters. Thus the algorithm, called PDHG-net-Ⅰ, can be formed as

$$\begin{cases} d_{n+1} = \frac{d_n + \sigma(A\bar{m}_n - f)}{1+\sigma} \\ m_{n+1} = \Lambda(m_n - \tau A^T d_{n+1}) \\ \bar{m}_{n+1} = m_{n+1} + \theta(m_{n+1} - m_n) \end{cases} \quad (7)$$

The parameters σ, τ and θ and the operator Λ are all learned by the network. The PDHG-net-Ⅰ learns the regularization functions including transform and regularier through the network implicitly.

PDHG-net-Ⅱ

If the constraint of data consistency $\|Am - f\|_2^2$ in problem (2) is relaxed as $F(Am, f)$ as in model (3), then F^* in the solution (4) is the convex conjugate of the function $F(Am, f)$. Followed by the PDHG-net-Ⅰ, a learned operator Γ is also used to replace $prox_{\sigma}[F^*]$, and the new algorithm, PDHG-net-Ⅱ, can be written as

$$\begin{cases} d_{n+1} = \Gamma(d_n + \sigma A\bar{m}_n, f) \\ m_{n+1} = \Lambda(m_n - \tau A^T d_{n+1}) \\ \bar{m}_{n+1} = m_{n+1} + \theta(m_{n+1} - m_n) \end{cases} \quad (8)$$

The primal proximal Λ, dual proximal Γ, parameters σ, τ and θ are all learned from training data. To improve the representation capacity of the network, the parameters of the network in each iteration are different, which makes the network a cascading architecture.

PDHG-net-Ⅲ

To utilize the learning ability of deep networks better and further improve the reconstruction quality based on PDHG-net-Ⅱ, the explicitly enforced updating structures $d_n + \sigma A\bar{m}_n$, $m_n - \tau A^* d_{n+1}$ were broken and the combinations of the variables were freely learned by the network. Instead of the hard acceleration step $m_{n+1} + \theta(m_{n+1} - m_n)$, the network can be designed to freely learn in what point the forward operator should be evaluated. Thus, the algorithm, called PDHG-net-Ⅲ, is formulated as

$$\begin{cases} d_{n+1} = \Gamma(d_n, Am_n, f) \\ m_{n+1} = \Lambda(m_n, A^T d_{n+1}) \end{cases} \quad (9)$$

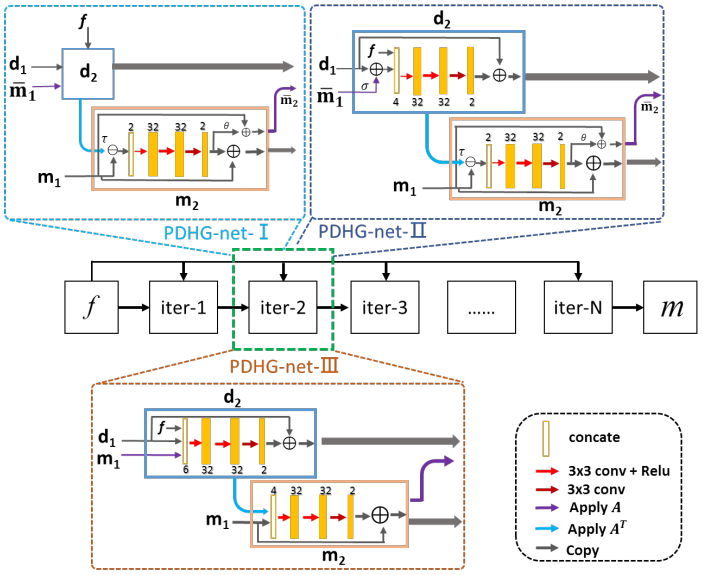


Fig 1. Architectures of the PDHG-nets.

② the ADMM approach

ADMM-net- Ⅰ

ADMM-net was designed by unrolling the Alternating Direction Method of Multipliers (ADMM) algorithm [24]. The original network, denoted as basic-ADMM-CSNet, learns the regularization parameters in the ADMM algorithm [20]. It was then generalized in their follow-up work, denoted as Generic-ADMM-CSNet [25] The improved network learns the image transformation and regularizer in the regularization function. Here, the Generic-ADMM-CSnet (called ADMM-net- Ⅰ hereafter) was used as the example.

In the context of ADMM-net- Ⅰ, the regularization term in model (2) is written as

$$\lambda R(m) = \sum_{l=1}^{L} \lambda_l \left\| \psi_l m \right\|_{\mathrm{p}} \qquad (10)$$

where ψ_l denotes a transformation matrix (e.g., discrete wavelet transform for a sparse representation), λ_l is the regularization parameter.

Introducing a set of independent auxiliary variables $z = \{z_1, z_2, \cdots, z_L\}$ in the spatial domain, ADMM reconstructs the image by solving the following subproblems:

$$\begin{cases} \underset{m}{\operatorname{argmin}} \dfrac{1}{2} \left\| Am - f \right\|_2^2 + \dfrac{\rho}{2} \left\| m + \beta - z \right\|_2^2 \\ \underset{z}{\operatorname{argmin}} \displaystyle\sum_{l=1}^{L} \lambda_l \left\| \psi_l z \right\|_{\mathrm{p}} + \dfrac{\rho}{2} \left\| m + \beta - z \right\|_2^2 \\ \underset{\beta}{\operatorname{argmin}} \displaystyle\sum_{l=1}^{L} \langle \beta, m - z \rangle \end{cases} \qquad (11)$$

The solution is

$$\begin{cases} M^{(n)}: m^{(n)} = \dfrac{\left[\mathrm{A}^T f + \rho\left(z^{(n-1)} - \beta^{(n-1)}\right)\right]}{\left(\mathrm{A}^T A + \rho I\right)} \\ Z^{(n)}: z^{(n)} = \mu_1 z^{(n,k-1)} + \mu_2\left(m^{(n)} + \beta^{(n-1)}\right) \\ \qquad\qquad - \sum_{l=1}^{L} \widetilde{\lambda_l}\, \psi_l^T H\left(\psi_l z^{(n,k-1)}\right) \\ P^{(n)}: \beta^{(n)} = \beta^{(n-1)} + \tilde{\eta}\left(m^{(n)} - z^{(n)}\right) \end{cases} \tag{12}$$

where $H(\cdot)$ refers to a non-linear operation corresponding to the gradient of the regularizer $\|\cdot\|_{\mathrm{p}}$. The second subproblem is solved approximately by directly employing the gradient descent algorithm, in which the iteration is indexed by k. In Eq. (12), all parameters $(\rho, \mu_1, \mu_2, \lambda_l, \tilde{\eta})$ are learnable and the transformations $\left(\psi_l, \psi_l^T\right)$, which are implemented linearly by convolving with kernels, as well as the nonlinear operator H, which is implemented by non-linear function ReLU in our experiments, are also learnable.

ADMM-net-Ⅱ

In Eq. (11), the sparse regularization term is learnable whereas the data consistency is measured by the L2 norm of the difference between the estimated and the acquired data at the sampled locations. It would be more accurate if the consistency in k-space is learned by the network from the training data as in model (3). With the ADMM algorithm, we propose to solve the model (3) with the regularization term (10) as follows:

$$\begin{cases} \underset{m}{\operatorname{argmin}}\, F(Am, f) + \dfrac{\rho}{2}\|m + \beta - z\|_2^2 \\ \underset{z}{\operatorname{argmin}} \displaystyle\sum_{l=1}^{L} \lambda_l \|\psi_l z\|_{\mathrm{p}} + \dfrac{\rho}{2}\|m + \beta - z\|_2^2 \\ \underset{\beta}{\operatorname{argmin}} \displaystyle\sum_{l=1}^{L} \langle \beta, m - z \rangle \end{cases} \tag{13}$$

Inspired by the solution to the second subproblem in (11), the solution to (13) is as follows:

$$\begin{cases} M^{(n)}: m^{(n)} = \gamma_1 m^{(n,k-1)} + \gamma_2\left(z^{(n)} - \beta^{(n-1)}\right) - A^T \Gamma\left(Am^{(n,k-1)}, f\right) \\ Z^{(n)}: z^{(n)} = \mu_1 z^{(n,k-1)} + \mu_2\left(m^{(n)} + \beta^{(n-1)}\right) - \displaystyle\sum_{l=1}^{L} \widetilde{\lambda_l}\, \psi_l^T H\left(\psi_l z^{(n,k-1)}\right) \\ P^{(n)}: \beta^{(n)} = \beta^{(n-1)} + \tilde{\eta}\left(m^{(n)} - z^{(n)}\right) \end{cases} \tag{14}$$

where $\Gamma(Am, f)$, which is accomplished by the neural network, refers to the function corresponding to the deviation of data consistency $F(Am, f)$.

ADMM-net-Ⅲ

In ADMM-net-Ⅱ, sparse prior is imposed as the prior information, with the powerful learning ability of deep networks, the prior besides sparsity could be learned from the training data, thus the reconstruction model, as listed in (3), becomes more general.

The second subproblem in (13) then becomes

$$\underset{z}{\operatorname{argmin}} R(z) + \frac{\rho}{2}\|m + \beta - z\|_2^2 \qquad (15)$$

Noticed that (15) is the same as (5), which is the proximal operator that can be replaced by a learned network. Followed the strategy of developing PDHG-net-III, we propose to freely learn the combinations of variables in the first subproblem of (13) by the network. So the solution iterations can be written as

$$\begin{cases} D^{(n)}: d^{(n)} = \Gamma(Am^{(n-1)}, f) \\ M^{(n)}: m^{(n)} = \Pi(m^{(n-1)}, z^{(n-1)} - \beta^{(n-1)}, \mathrm{A}^T d^{(n)}) \\ Z^{(n)}: z^{(n)} = \Lambda\left(m^{(n)} + \beta^{(n-1)}\right) \\ P^{(n)}: \beta^{(n)} = \beta^{(n-1)} + \tilde{\eta}\left(m^{(n)} - z^{(n)}\right) \end{cases} \qquad (16)$$

The operator Γ, Π, Λ and the parameter $\tilde{\eta}$ are all learned by the network.

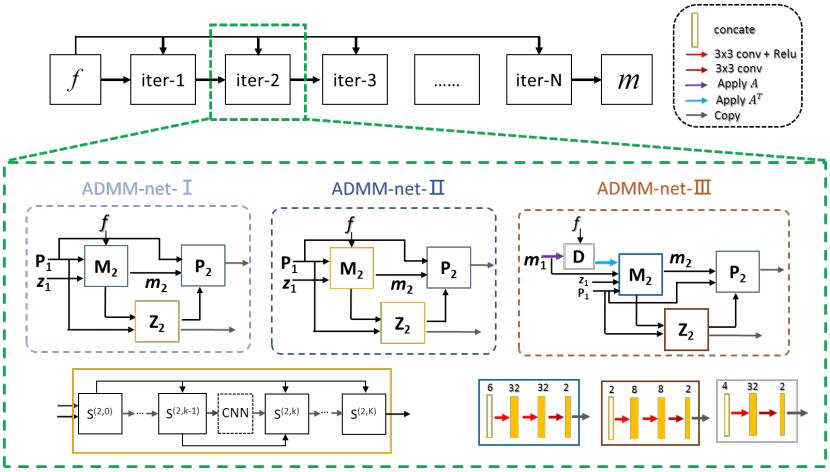


Fig 2. Architectures of the ADMM-nets.

③ the ISTA approach

ISTA-net- Ⅰ

Iterative shrinkage-thresholding algorithm (ISTA) is a popular first-order method to solve linear inverse problem [26]. For the CS reconstruction problem (2) with the regularization $\|\Psi m\|_1$, ISTA reconstructs the images with following iterations:

$$\begin{cases} r^{(n+1)} = m^{(n)} - \rho \mathrm{A}^T\left(\mathrm{A}m^{(n)} - f\right) \\ m^{(n+1)} = \underset{m}{\operatorname{argmin}} \frac{1}{2}\left\|m - r^{(n+1)}\right\|_2^2 + \tau\|\Psi m\|_1 \end{cases} \qquad (18)$$

In ISTA-net- Ⅰ, a general nonlinear transform function G is adopted to sparsify the images, whose parameters are learnable. Therefore, iteration (18) becomes

$$\begin{cases} r^{(n+1)} = m^{(n)} - \rho \mathrm{A}^T\left(\mathrm{A}m^{(n)} - f\right) \\ m^{(n+1)} = \underset{m}{\operatorname{argmin}} \frac{1}{2}\left\|G(m) - G(r^{(n+1)})\right\|_2^2 + \tau\|\mathrm{G}(m)\|_1 \end{cases} \quad (19)$$

The solution is

$$\begin{cases} r^{(n+1)} = m^{(n)} - \rho \mathrm{A}^T\left(\mathrm{A}m^{(n)} - f\right) \\ m^{(n+1)} = \tilde{G}\left(soft\left(G\left(r^{(n+1)}\right), \theta\right)\right) \end{cases} \quad (20)$$

the step size ρ, shrinkage threshold θ, forward transform G and the backward transform $\tilde{G}$ are the learnable parameters in ISTA-net-Ⅰ.

ISTA-net-Ⅱ

Based on the ISTA-net-Ⅰ, we further relax the data consistency term $\|Am - f\|_2^2$ as $F(Am, f)$, then the deviation of $F(Am, f)$ can be written as $A^T\Gamma(Am, f)$, in which the function $\Gamma(Am, f)$ can be accomplished by the deep network. Therefore, the iteration of ISTA-net-Ⅱ becomes

$$\begin{cases} d^{(n+1)} = \Gamma\left(\mathrm{A}m^{(n)}, f\right) \\ r^{(n+1)} = m^{(n)} - \rho \mathrm{A}^T d^{(n+1)} \\ m^{(n+1)} = \tilde{G}\left(soft\left(G\left(r^{(n+1)}\right), \theta\right)\right) \end{cases} \quad (21)$$

ISTA-net-Ⅲ

In ISTA, the residual $r^{(n+1)}$ is imposed by the difference between the current solution and the deviation of data consistency term, we then propose to use the network to learn the combination of these variables. Thus the solution is as follows:

$$\begin{cases} d^{(n+1)} = \Gamma\left(\mathrm{A}m^{(n)}, f\right) \\ r^{(n+1)} = \Lambda(m^{(n)}, A^T d^{(n+1)}) \\ m^{(n+1)} = \tilde{G}\left(soft\left(G\left(r^{(n+1)}\right), \theta\right)\right) \end{cases} \quad (22)$$

The operators Γ, Λ, G and $\tilde{G}$ are all realized by networks.

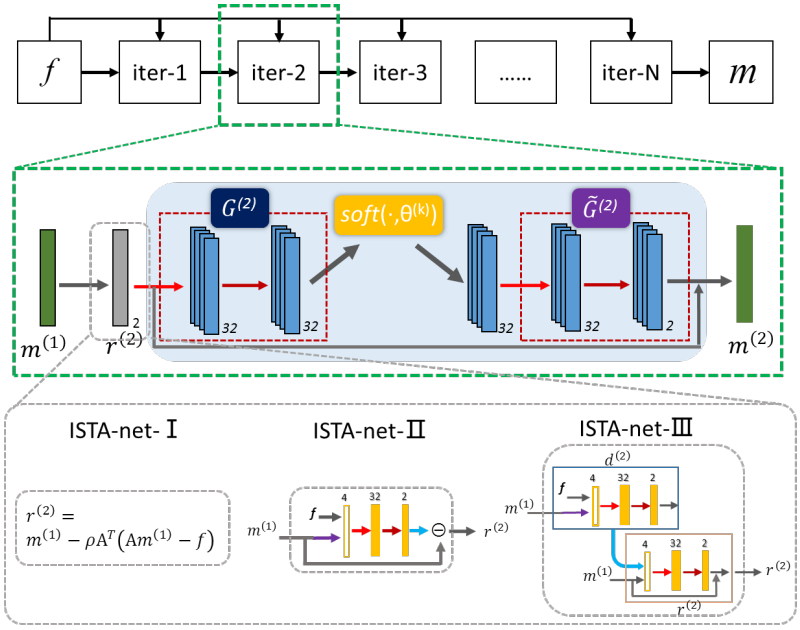


Fig 3. Architectures of the ISTA-nets.

3. Method

3.1 Network architecture

The network architectures of each algorithm mentioned above are derived from the data flow of the original optimization methods. The convolutions in our paper are all 3×3 pixels in size, and the nonlinear operator is chosen to be Rectified Linear Unites (ReLU). As the data consistency is realized by the neural network, algorithm of state Ⅱ is deeper than state Ⅰ for each approach. The output of each CNN block has two channels representing the real and imaginary parts as MR data is complex-valued.

The entire architecture of primal dual networks and one iteration block of the three states of PDHG-net are illustrated in Fig. 1. The primal and dual iterations have the same architecture with three convolutional layers in each block of PDHG-net-Ⅱ and PDHG-net-Ⅲ. To train the network more easily, residual network was used. For PDHG-net-Ⅱ, the number of channels is 2-32-32-2 in each primal update and 4-32-32-2 in each dual update, whereas for PDHG-net-Ⅲ, the number of channels is 4-32-32-2 in each primal update and 6-32-32-2 in each dual update. We set the number of iterations to be 10 in all three networks.

The data flow graphs of the ADMM networks for one iteration are demonstrated in Fig. 2. The graph nodes of ADMM-net-Ⅰ, ADMM-net-Ⅱ and ADMM-net-Ⅲ correspond to the operations in Eq. (11), Eq. (14) and Eq. (17), respectively. For ADMM-net-Ⅰ, the operation $\tilde{\lambda}_l D_l^T H\left(D_l z^{(n,k-1)}\right)$ in $Z^{(n)}$ is accomplished by a CNN module, which comprises of two convolution layers and a non-linear activation layer with 8 filters. The reconstruction module $M^{(n)}$ in ADMM-net-Ⅱ is as the same structure to $Z^{(n)}$, but with 32 filters. The number of iterations for the ADMM-nets are all 15 as suggested in the original ADMM-net-Ⅰ work [25].

The second iteration of ISTA-nets is illustrated in Fig. 3. To give a better reconstruction, the image was sparsified in the residual domain, which leads to a sparser representation and make it a residual network to facilitate the training. The number of filters we used for ISTA-net-Ⅰ is 32. In ISTA-net-Ⅱ, $\Gamma\left(\mathrm{A}m^{(n)}, f\right)$ in Eq. (21) is modeled as two convolution operators and one ReLU operator. 10 iterations were used here for ISTA-nets.

3.2 Data acquisition

Training data

Overall 2100 fully sampled multi-contrast data from 10 subjects with a 3T scanner (MAGNETOM Trio, SIEMENS AG, Erlangen, Germany) were collected and informed consent was obtained from the imaging object in compliance with the IRB policy. The fully sampled data was acquired by a 12-channel head coil with matrix size of 256×256 and adaptively combined to single-channel data [27] and then retrospectively undersampled using Poisson disk sampling mask.

Testing data

We tested the proposed methods on 398 human brain 2D slices from 3D data acquired from SIEMENS 3T scanner with 32-channel head coil and 3D T1-weighted SPACE sequence, TE/TR=8.4/1000ms, FOV=25.6×25.6×25.6cm^3. The data was fully acquired and then manually down-sampled for reconstruction.

The proposed methods also have been tested on the fully sampled data from other commercial 3T scanners (GE Healthcare, Waukesha, WI; United Imaging Healthcare, Shanghai, China).

3.3 Evaluation

In network training, the mean square error (MSE) is chosen as the loss function. Given pairs of training data, the loss between the network output and ground truth is defined as

$$L_{MSE}(\Theta) = \frac{1}{N}\sum_{i=1}^{N}\left\|\hat{m}(\Theta, f) - m^{ref}\right\|_2^2 \qquad (23)$$

where $\hat{m}(\Theta, f)$ is the network output based on network parameter Θ and undersampled k-space data f, m^{ref} is the corresponding ground truth. Specifically, because of the symmetric constraint in the ISTA-nets, the loss function in ISTA-nets is designed as follows:

$$L(\Theta) = L_{MSE}(\Theta) + \gamma L_{constraint}(\Theta) \qquad (24)$$

where $L_{MSE}(\Theta)$ is defined as (23) and $L_{constraint}(\Theta)$ is imposed to satisfy the symmetric constraint, which is defined as

$$L_{constraint}(\Theta) = \frac{1}{N}\sum_{i=1}^{N}\sum_{k=1}^{N_p}\left\|\tilde{G}^{(k)}\left(G^{(k)}(\hat{m})\right) - \hat{m}\right\|_2^2 \qquad (25)$$

where N_p is the total number of iterations. In our experiments, $N_p = 10, \gamma = 0.01$.

Several similarity metrics, including MSE, SSIM and PSNR, were used to compare the

reconstruction results of different methods with the reference image from fully sampled data.

We trained the networks by minimizing the loss function defined above using the ADAM optimizer in TensorFlow. And the trainings were performed on an Ubuntu 16.04 LTS (64-bit) operating system equipped with a Tesla TITAN Xp Graphics Processing Unit (GPU, 12GB memory) with CUDA and CUDNN support.

4. Result

As the constraints in the specific model (1) are gradually relaxed, the quality of the reconstruction gets better and better, which is shown in Fig. 4. From the state Ⅰ to the state Ⅲ, the reconstruction model becomes more general, which is beneficial for the network to learn the property of the training data, including but not limited to sparsity, thus improves the image quality. Nevertheless, the required training set is expected to increase for achieving the optimal performance because of the increasing number of parameters to be learned.

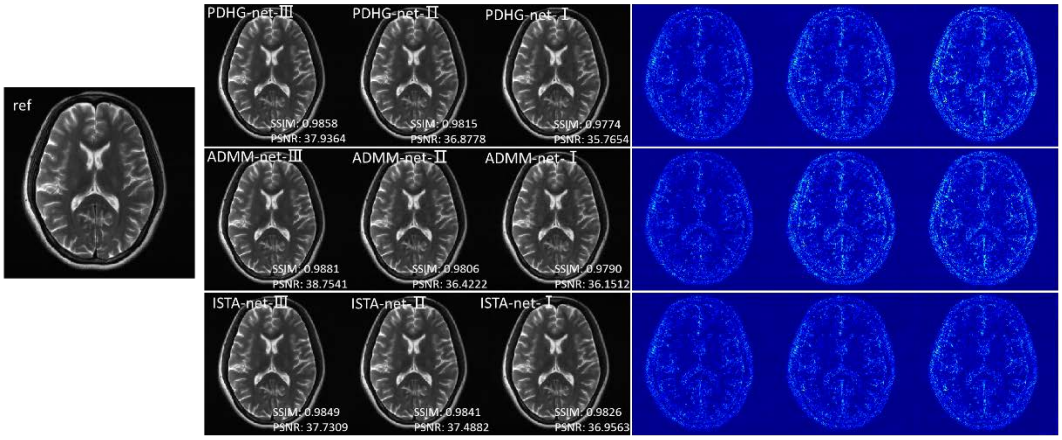


Fig 4. Reconstruction results and the corresponding error maps when gradually relaxing constraints with respective to the three algorithms. A 10x Poisson disk sampling mask was used on an axial data from the UIH scanner.

Fig 5 shows the visual comparisons with the acceleration factor of 6. The zoom-in images of the enclosed part and the corresponding error maps as well as the quantitative metrics are also provided. With the constraints relaxed, the fine details are able to be recovered, as the prior information is learned from the training data, which is more suitable than the hand-designed prior for the undersampled data.

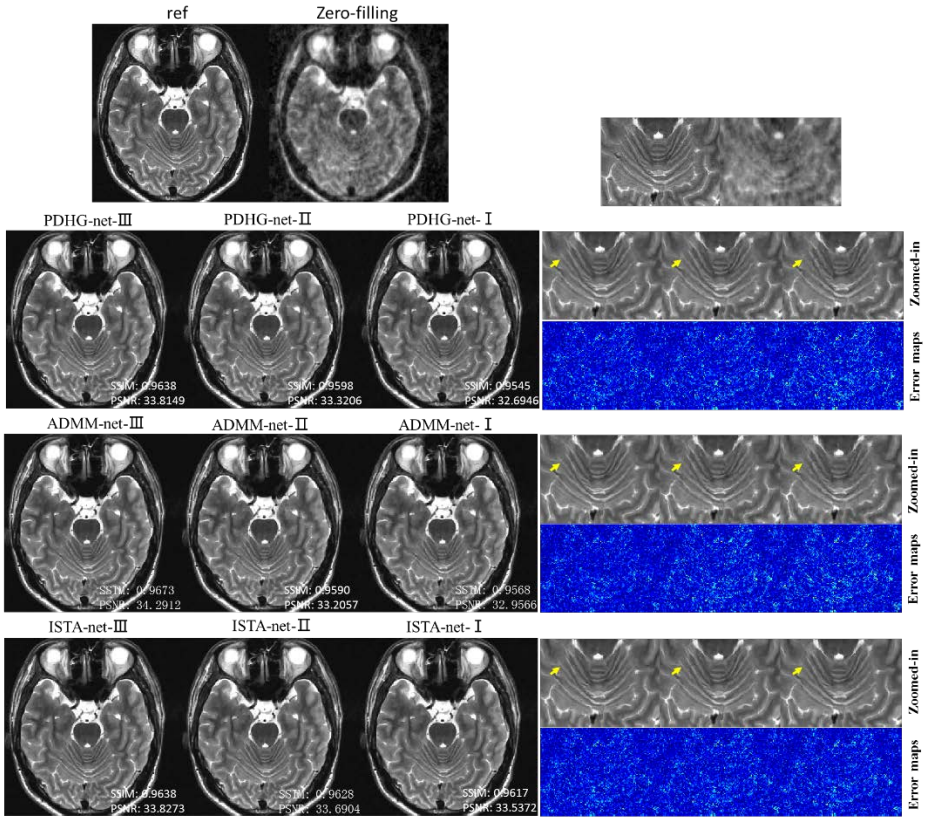


Fig 5. Reconstruction results with a 6x Poisson disk sampling on an axial data from the Siemens scanner. The zoomed in images and the corresponding error maps are provided on the right, respectively.

5. Discussion

5.1 Training set

Deep learning methods achieve superior performance heavily relying on the large training dataset. For MR reconstruction, data-driven methods usually demand more training data than model-driven methods. Since the solution space is huge without model, data-driven methods search the mapping between the training pairs on the large dataset to prevent the solution from local minimum, which is the issue of overfitting. Whereas for model-driven methods, the solution space is narrowed by the reconstruction model, and the solution searching is guided by the iterative inference algorithm, thus the training data for model-driven methods is reduced.

In this paper, we gradually relax the requirements on a specific reconstruction model (e.g. CS model). With more uncertainty in the model, that is increasing the degree of freedom of the network, the size of training data is expected to be increased for achieving the optimal performance. As shown in Fig. 6, with little training data, the method with more relaxed constraints (state Ⅲ) has comparable performance or even worse than the methods with less

relaxed constraints (states Ⅰ and Ⅱ). As the training data increases, the performance of state Ⅲ changes more significantly than others. With sufficient training data, state Ⅲ gives the best reconstruction.

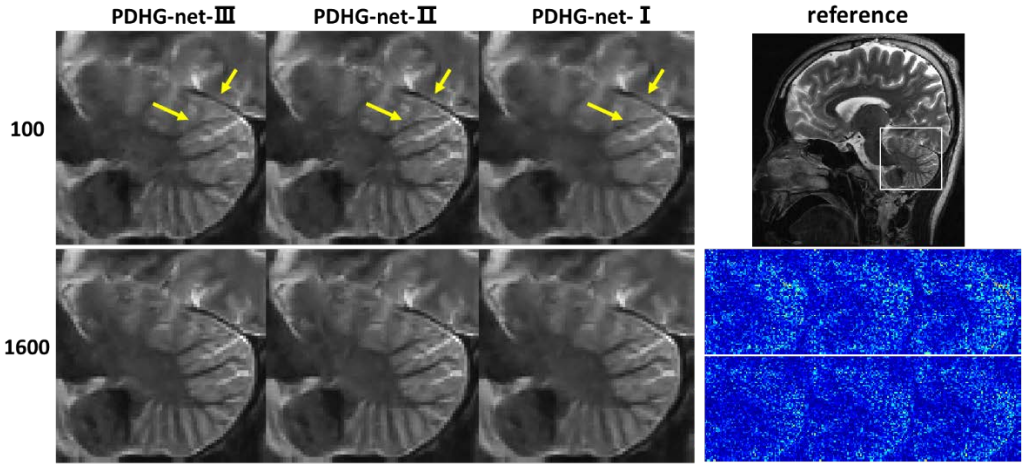


Fig 6. The reconstructed zoom-in images of the enclosed part with a 6x Poisson disk sampling on a sagittal data from the Siemens scanner. The results with a small training size are located in the first row on the left and the second row shows the results with more training data. The corresponding error maps of the enclosed part are also provided on the right bottom.

5.2 Stability and reconstruction accuracy

The stability of the network is an important factor to be considered in practice. Given that the network is trained with a specific sampling pattern, the question is how robust the trained network with respect to the changes of acceleration factor is. In our experiments, all the networks are trained with the 6-fold Poisson disk sampling mask. We have tested the performance of the networks with other sampling ratios, shown in the Fig. 7. The results show the flexibility of the networks for changing the amount of acquired data. The quality of reconstruction deteriorates with less samples for each state, whereas for the fixed acceleration, the improvement of quality induced by relaxing can be observed. Moreover, the average reconstruction time with R=6 are listed in Table 2.

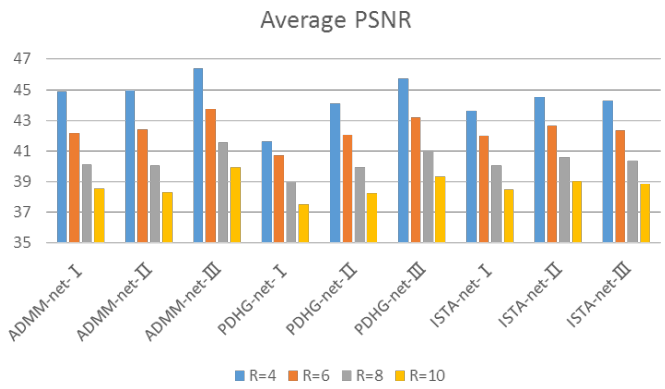


Fig 7. The average PSNR performance of the all networks with different acceleration factors.

Table 2. Average reconstruction time comparison between the methods.

	Ⅰ	Ⅱ	Ⅲ
PDHG-net	0.03517s	0.03904s	0.03685s
ADMM-net	0.12252s	0.15485s	0.14938s
ISTA-net	0.03511s	0.03741s	0.03850s

CS-based approaches suffer from detail loss at large acceleration factors, several attempts have been made to address this issue [28, 29]. Although deep learning reconstruction is superior to CS, it still exhibits feature loss as CS does due to the l2-norm loss function, which is employed by most DL approaches. In this paper, the results are with higher quality in terms of various quantitative values compared with the original version, but still exhibit over smoothing at high frequency region. Figure 8 shows the error spectrum plots (ESP) [30] with Fourier radial of the three algorithms with the 6x sagittal data from GE scanner. From the ESP, the relative error increases as the Fourier radial increases, which indicates that the high frequency part of the image has higher error than low frequency part. In the specific algorithm, the network with state Ⅲ has the lowest error. This is consistent with the visual comparison.

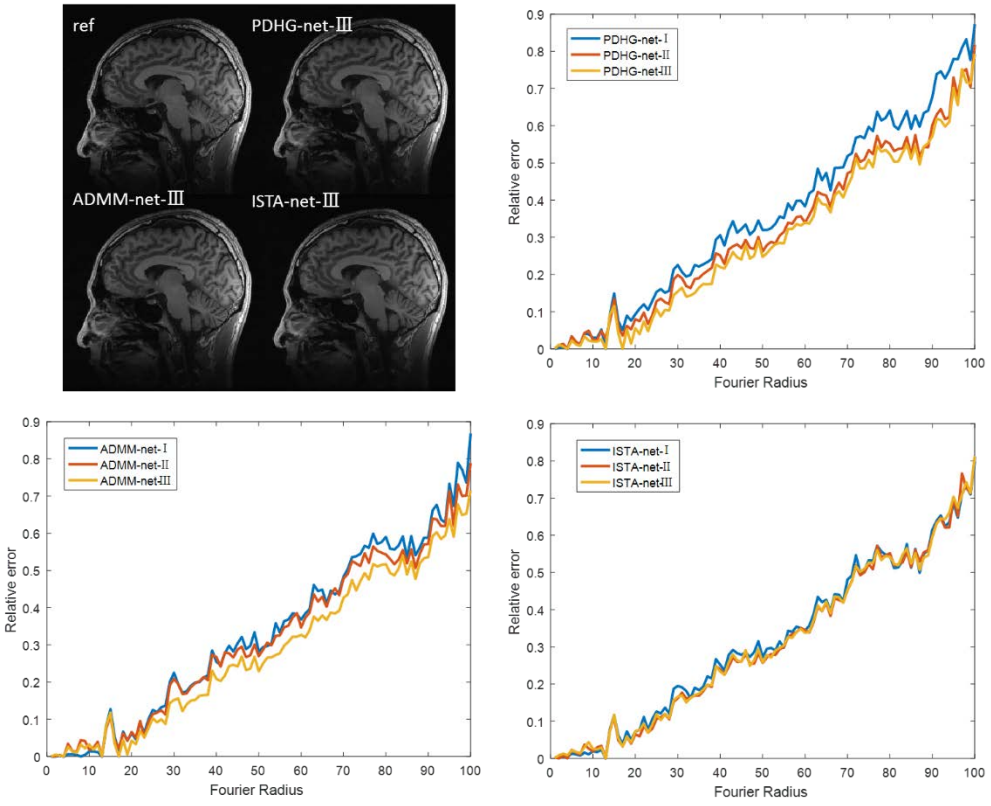


Fig 8. Error Spectrum Plots of the three types of algorithms.

In our experiments, the sub-network architectures and the parameters of the same module in all three states are the same to give a fair comparison. Another consideration is whether the improvement from state Ⅰ to state Ⅱ is induced by the learned data fidelity rather than the deeper network. We have added convolutional layers to the primal modules of PDHG-net-Ⅰ to make it have the same number of parameters as PDHG-net-Ⅱ, the new network was denoted as PDHG-net-Ⅰ*. The average PSNR performance and the visual comparison on the 6x testing data are shown in Fig. 9 and Fig. 10, respectively. PDHG-net-Ⅰ* performs better than PDHG-net-Ⅰ because of the deeper network with more learning parameters, whereas it is not comparable to PDHG-net-Ⅱ, the reason is that the learned data fidelity is more suitable than the predefined l2-norm for the data.

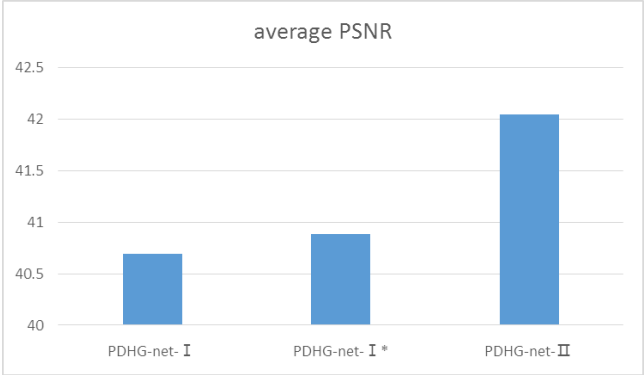


Fig 9. The effectiveness of learned data fidelity. PDHG-net-Ⅰ* has the same structure as PDHG-net-Ⅰ but the same number of parameters as PDHG-net-Ⅱ.

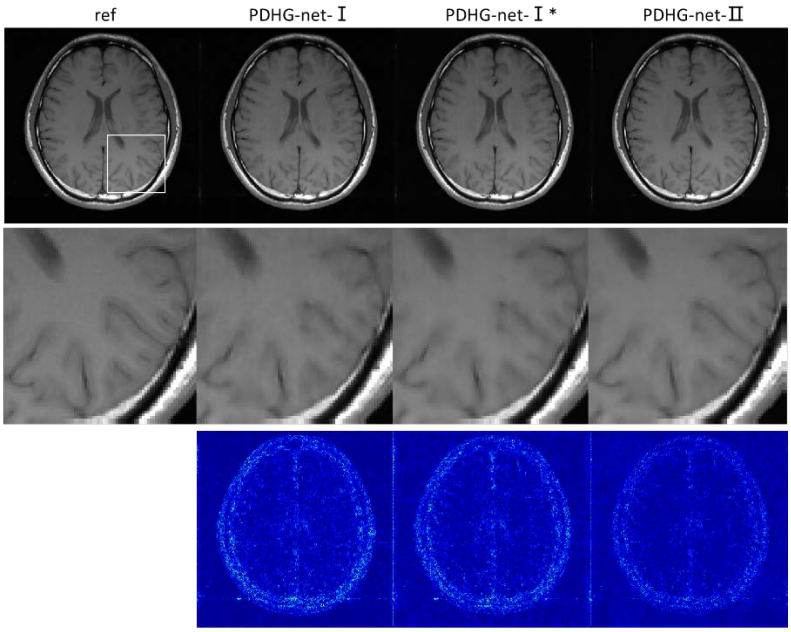


Fig 10. Reconstruction results with a 6x Poisson disk sampling on an axial data from the GE scanner.

5.3 Network interpretation

For linear inverse problem, signal priors are often used to regularize the inverse problem. Traditionally, these priors are hand-designed based on empirical observations of images such as transform sparsity. Though these priors can be used in many inverse problems related to images and usually have efficient solvers, they may have poor performance on a specific problem. For an individual problem like image reconstruction, hand-crafted priors are too general to constraint the solution set, learning can fit the data property better if the testing data is in the same type of training data. That's why learning-based methods perform better than traditional methods.

For the model-driven deep learning methods, the sub-network at each iteration is designed with the data flow graphs, which are derived from the iterative procedure of the optimization algorithm. Although the networks of state Ⅲ have little constraints in the model and inference, they indeed root from the corresponding mathematical algorithms with the module of network being the same as the data flow graphs of the inferences. The network, especially the convolutional neural network used here, is adopted to parameterize the solution space due to the strong representative ability, in order to make the inference more suitable for the specific applications.

5.4 Open issues in DL reconstruction

Although the optimization algorithm induced networks can learn the parameters in the algorithm and achieve superior performance, developing network architectures is still a time-consuming and error prone process, since all the hyper-parameters of the network such as learning rate and number of feature maps are decided empirically. In our experiments, the hyper-parameters of the networks in one algorithm chain are the same for fair comparison. For example, the learning rate, number of iterations, number of layers and the feature maps of the same module are set to be the same.

Recently, network architecture search (NAS) is considered as a feasible and promising tool to automatically search for the optimal network architecture [31]. Several novel NAS methods, such as reinforcement learning and evolutionary computation, have been developed and applied in a variety of deep learning tasks [32-34]. It also can be applied in MR image reconstruction in the future.

Besides the hyper-parameters, loss function is another important factor need to be considered in network design. Loss function guides the learning direction, and different loss functions may result in different reconstructions. The MSE we used here is prone to fail to recover tiny structures in the images, as MSE is an average indicator of the whole image, more advanced loss functions related to the integrant of interest could be applied [35].

6. Conclusion

In this paper, we developed an effective framework to integrate classical inference and deep neural network to maximize the potential of deep learning and model-based reconstruction for

fast MR imaging. The experimental results on in vivo data demonstrate the effectiveness of the proposed framework. This work attempts to provide a guideline on how to improve the image quality with deep learning based on the traditional reconstruction algorithms. More techniques and properties of the unification of deep learning and traditional reconstruction methods should be investigated in the future.

Reference

[1] G. Mcgibney, M. R. Smith, S. T. Nichols, and A. Crawley, "Quantitative-Evaluation of Several Partial Fourier Reconstruction Algorithms Used in MRI," *Magnetic Resonance in Medicine,* vol. 30, pp. 51-59, Jul 1993.

[2] K. P. Pruessmann, M. Weiger, M. B. Scheidegger, and P. Boesiger, "SENSE: Sensitivity encoding for fast MRI," *Magnetic Resonance in Medicine,* vol. 42, pp. 952-962, Nov 1999.

[3] M. A. Griswold, P. M. Jakob, R. M. Heidemann, M. Nittka, V. Jellus, J. M. Wang*, et al.*, "Generalized Autocalibrating Partially Parallel Acquisitions (GRAPPA)," *Magnetic Resonance in Medicine,* vol. 47, pp. 1202-1210, Jun 2002.

[4] M. Lustig, D. Donoho, and J. M. Pauly, "Sparse MRI: The application of compressed sensing for rapid MR imaging," *Magnetic Resonance in Medicine,* vol. 58, pp. 1182-1195, Dec 2007.

[5] D. Liang, B. Liu, J. J. Wang, and L. Ying, "Accelerating SENSE Using Compressed Sensing," *Magnetic Resonance in Medicine,* vol. 62, pp. 1574-1584, Dec 2009.

[6] S. Ravishankar and Y. Bresler, "MR image reconstruction from highly undersampled k-space data by dictionary learning," *IEEE Trans Med Imaging,* vol. 30, pp. 1028-41, May 2011.

[7] Q. Liu, S. Wang, L. Ying, X. Peng, Y. Zhu, and D. Liang, "Adaptive Dictionary Learning in Sparse Gradient Domain for Image Recovery," *IEEE Transactions on Image Processing,* vol. 22, pp. 4652-4663, Dec 2013.

[8] P. Hansen, *Rank-Deficient and Discrete Ill-Posed Problems*. Philadelphia: SIAM, 1998.

[9] X. Zhu and P. Milanfar, "Automatic Parameter Selection for Denoising Algorithms Using a No-Reference Measure of Image Content," *Ieee Transactions on Image Processing,* vol. 19, pp. 3116-3132, Dec 2010.

[10] S. Wang, Z. Su, L. Ying, X. Peng, S. Zhu, F. Liang*, et al.*, "Accelerating Magnetic Resonance Imaging via Deep Learning," *IEEE Conference on International Symposium on Biomedical Imaging (ISBI),* pp. 514-517, 2016.

[11] B. Zhu, J. Z. Liu, S. F. Cauley, B. R. Rosen, and M. S. Rosen, "Image reconstruction by domain-transform manifold learning," *Nature,* vol. 555, pp. 487-492, Mar 21 2018.

[12] T. Eo, Y. Jun, T. Kim, J. Jang, H. J. Lee, and D. Hwang, "KIKI-net: cross-domain convolutional neural networks for reconstructing undersampled magnetic resonance images," *Magn Reson Med,* vol. 80, pp. 2188-2201, Nov 2018.

[13] J. Schlemper, J. Caballero, J. V. Hajnal, A. N. Price, and D. Rueckert, "A Deep Cascade of Convolutional Neural Networks for Dynamic MR Image Reconstruction," *IEEE Trans Med Imaging,* vol. 37, pp. 491-503, Feb 2018.

[14] T. M. Quan, T. Nguyen-Duc, and W. K. Jeong, "Compressed Sensing MRI Reconstruction Using a Generative Adversarial Network With a Cyclic Loss," *IEEE Transactions on Medical Imaging,* vol. 37, pp. 1488-1497, Jun 2018.

[15] Y. Han, J. Yoo, H. H. Kim, H. J. Shin, K. Sung, and J. C. Ye, "Deep learning with domain

adaptation for accelerated projection-reconstruction MR," *Magn Reson Med,* vol. 80, pp. 1189-1205, Sep 2018.

[16] M. Mardani, E. Gong, J. Y. Cheng, S. S. Vasanawala, G. Zaharchuk, L. Xing*, et al.*, "Deep Generative Adversarial Neural Networks for Compressive Sensing MRI," *IEEE Trans Med Imaging,* vol. 38, pp. 167-179, Jan 2019.

[17] G. Yang, S. M. Yu, H. Dong, G. Slabaugh, P. L. Dragotti, X. J. Ye*, et al.*, "DAGAN: Deep De-Aliasing Generative Adversarial Networks for Fast Compressed Sensing MRI Reconstruction," *IEEE Transactions on Medical Imaging,* vol. 37, pp. 1310-1321, Jun 2018.

[18] M. Akcakaya, S. Moeller, S. Weingartner, and K. Ugurbil, "Scan-specific robust artificial-neural-networks for k-space interpolation (RAKI) reconstruction: Database-free deep learning for fast imaging," *Magnetic Resonance in Medicine,* vol. 81, pp. 439-453, Jan 2019.

[19] H. K. Aggarwal, M. P. Mani, and M. Jacob, "MoDL: Model-Based Deep Learning Architecture for Inverse Problems," *IEEE Trans Med Imaging,* vol. 38, pp. 394-405, Feb 2019.

[20] Y. Yang, J. Sun, H. Li, and Z. Xu, "Deep ADMM-Net for Compressive Sensing MRI," *Neural Information Processing Systems,* pp. 10-18, 2016.

[21] C. Qin, J. Schlemper, J. Caballero, A. N. Price, J. V. Hajnal, and D. Rueckert, "Convolutional Recurrent Neural Networks for Dynamic MR Image Reconstruction," *IEEE Trans Med Imaging,* vol. 38, pp. 280-290, Jan 2019.

[22] K. Hammernik, T. Klatzer, E. Kobler, M. P. Recht, D. K. Sodickson, T. Pock*, et al.*, "Learning a variational network for reconstruction of accelerated MRI data," *Magnetic Resonance in Medicine,* vol. 79, pp. 3055-3071, Jun 2018.

[23] A. Chambolle and T. Pock, "A First-Order Primal-Dual Algorithm for Convex Problems with Applications to Imaging," *Journal of Mathematical Imaging and Vision,* vol. 40, pp. 120-145, Mar 2011.

[24] S. Boyd, N. Parikh, E. Chu, B. Peleato, and J. Eckstein, "Distributed Optimization and Statistical Learning via the Alternating Direction Method of Multipliers," *Foundations and Trends in Machine Learning,* vol. 3, pp. 1-122, 2011.

[25] Y. Yang, J. Sun, H. Li, and Z. Xu, "ADMM-CSNet: A Deep Learning Approach for Image Compressive Sensing," *IEEE Trans Pattern Anal Mach Intell,* Nov 28 2018.

[26] A. Beck and M. Teboulle, "A Fast Iterative Shrinkage-Thresholding Algorithm for Linear Inverse Problems," *Siam Journal on Imaging Sciences,* vol. 2, pp. 183-202, 2009.

[27] D. O. Walsh, A. F. Gmitro, and M. W. Marcellin, "Adaptive reconstruction of phased array MR imagery," *Magnetic Resonance in Medicine,* vol. 43, pp. 682-690, May 2000.

[28] J. Cheng, S. Jia, L. Ying, Y. Y. Liu, S. S. Wang, Y. J. Zhu*, et al.*, "Improved parallel image reconstruction using feature refinement," *Magnetic Resonance in Medicine,* vol. 80, pp. 211-223, Jul 2018.

[29] S. S. Wang, J. B. Liu, Q. G. Liu, L. Ying, X. Liu, H. R. Zheng*, et al.*, "Iterative feature refinement for accurate undersampled MR image reconstruction," *Physics in Medicine and Biology,* vol. 61, pp. 3291-3316, May 7 2016.

[30] T. H. Kim and J. P. Haldar, "The Fourier Radial Error Spectrum Plot: A More Nuanced Quantitative Evaluation of Image Reconstruction Quality," *2018 IEEE 15th International Symposium on Biomedical Imaging (Isbi 2018),* pp. 61-64, 2018.

[31] T. Elsken, J. H. Metzen, and F. Hutter, "Neural Architecture Search: A Survey," *Journal of*

Machine Learning Research, vol. 20, 2019.

[32] P. Fonseca, J. Mendoza, J. Wainer, J. Ferrer, J. Pinto, J. Guerrero*, et al.*, "Automatic breast density classification using a convolutional neural network architecture search procedure," *Medical Imaging 2015: Computer-Aided Diagnosis,* vol. 9414, 2015.

[33] Y. Weng, T. B. Zhou, Y. J. Li, and X. Y. Qiu, "NAS-Unet: Neural Architecture Search for Medical Image Segmentation," *IEEE Access,* vol. 7, pp. 44247-44257, 2019.

[34] Y. Weng, T. B. Zhou, L. Liu, and C. L. Xia, "Automatic Convolutional Neural Architecture Search for Image Classification Under Different Scenes," *IEEE Access,* vol. 7, pp. 38495-38506, 2019.

[35] S. Wang, Z. Ke, H. Cheng, S. Jia, L. Ying, H. Zheng*, et al.*, "DIMENSION: Dynamic MR Imaging with Both K-space and Spatial Prior Knowledge Obtained via Multi-Supervised Network Training," *NMR in Biomedicine,* 2019.